Dielectric Analysis of the Breakup of Liquid Crystalline Polymer Fibers in a Thermoplastic Matrix

A. Boersma,* M. Wübbenhorst, and J. van Turnhout

Delft University of Technology, Faculty of Chemical Technology and Materials Science, Department of Polymer Technology, Julianalaan 136, 2628 BL Delft, The Netherlands

Received December 6, 1996; Revised Manuscript Received February 24, 1997[⊗]

ABSTRACT: In this paper we discuss the use of dielectric spectroscopy as a means to study the morphology of polymer blends. We have investigated a model system of thermotropic liquid crystalline polymer (Vectra B950) fibers lined up in a polypropylene (Stamylan P 13E10) matrix. The appearance of interfacial polarization at the interface between the two polymeric phases makes it possible to calculate the shape of the inclusions. For this purpose a formula is derived, which gives the shape factor of a distorted fiber as a function of the distortion amplitude. The calculated shapes of the fibers agree very well with the actual shapes, despite the approximations made. The agreement was proven by performing dielectric measurements under an optical microscope. As expected, the growth rate of thick fibers is smaller than that of thinner ones. A comparison between experiments under the microscope and in a dielectric sample holder showed the importance of the heating rate on the breakup of the fibers.

I. Introduction

Fiber-reinforced polymers receive a lot of attention in the literature. During the last decade, numerous articles about the in situ generation of reinforcing fibers have been published (for review articles see, e.g., Crevecoeur,[1] Roetting,[2] and Qin[3]). These self-reinforcing polymer composites consist of a liquid crystalline polymer (LCP) dispersed in a thermoplastic matrix. Due to the liquid crystalline nature of the polymer, the LCP phase forms fibers during the processing of these blends. One of the advantages of such blends over conventional short fiber-reinforced composites is the reduction of the viscosity during processing by the LCP fraction. While glass or carbon fibers can break, LCP fibers are formed during the processing step. The properties of the blends formed are determined by the composition, size, shape, and distribution of the LCP fraction in the thermoplastic matrix polymer (Qin[3]).

The morphology of the blend strongly depends on the processing conditions like blend composition, extrusion or injection molding conditions, and viscosity ratio of the polymers. Most articles in the literature discuss the influence of these processing conditions on the morphology (Heino[4]) and on the mechanical (O'Donnell[5]) and thermal (Choy[6]) properties of the formed blends. The influence of compatibilizers is also the subject of a number of articles (e.g., Datta,[7] O'Donnell[8]). Scanning electron microscopy (SEM) is usually used to determine the morphology. The problem with SEM is that it can only be done after formation of the blend. It would be desirable to follow the structure formation during processing. Dielectric analysis is a technique which can be exploited for this on-line morphology control. In this article we take a first step in investigating this by performing dielectric measurements on a model system of LCP fibers in a thermoplastic matrix.

In the past a number of articles are published about the dielectric properties of polymer blends. Some authors discuss the influence of the miscibility of the polymers on the position and broadness of the α-loss peak. The existence of two separate α-peaks indicates at least partial phase separation (Carius[9]). Rellick[10,11] attributes the broadening of the α-peak to an increase in phase separation, whereas Angeli[12] and Zetsche[13] attribute it to an improved miscibility of the two components. Other authors have considered the shape of the inclusions in their articles. Bánhegyi published a series of articles in which the influence of the shape of the inclusions is discussed.[14−17] Only a few authors used the Maxwell−Wagner−Sillars (MWS) or interfacial polarization in their research of polymeric blends. Maybe this is caused by a discouraging conversation of Anderson with Cole (Anderson[18]) about interfacial polarization. Daly[19] used the MWS polarization to investigate laminates. Hayward[20] performed dielectric measurements on a model system of conductive inclusions in a non conductive matrix in order to study the MWS polarization. The appearance of phase separation during the cure of thermoplastic modified epoxy resins was demonstrated by MacKinnon,[21] whereas Dionísio[22] used MWS polarization to prove the existence of phase separation in polymer blends. Steeman[23] compared the calculated shape of the inclusions to SEM micrographs and found that the calculated shape agreed well with the observed one.

In this article we utilize the effect of interfacial polarization to determine the shape of fibers during the breakup process in the molten state.

The stability of polymeric blends during processing is an important subject in the research of in-situ composites. Breakup experiments of polymer fibers in a polymer matrix have been used by a number of authors to investigate the stability of polymer blends (e.g., Machiels[24,25]). From the growth rate of the distortion it is possible to calculate the interfacial tension between the polymer phases (Elmendorp,[26] Elemans,[27] Watkins[28]). The interfacial tension has a large influence on the stability of polymer blends. This topic will be addressed in another paper (Boersma[29]).

There are several mechanisms by which a fiber can break up. Apart from the classical Rayleigh distortion (Lord Rayleigh,[30] Tomotika[31,32]), retraction and end-pinching (Stone[33]) are also possible breakup mechanisms. Machiels[24] showed that the breakup process of an LCP fiber in polypropylene is a combination of Rayleigh distortion, end-pinching, and retraction. However in the present paper we assume the breakup mechanism to be solely of the Rayleigh type, since the mathematical description of retraction and end-pinching are difficult to handle.

[⊗] Abstract published in *Advance ACS Abstracts,* April 1, 1997.

S0024-9297(96)01794-9 CCC: $14.00

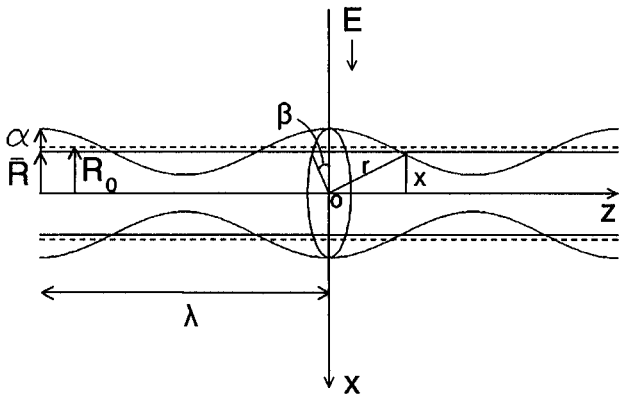

Figure 1. Sinusoidal distortion of a liquid cylinder. $R(z) = \bar{R} + \alpha \cos(2\pi z/\lambda)$. The electric field is directed in the x-direction. R_0 is the radius of the undisturbed thread.

II. Theory

Determination of the Shape Factor. Dielectric analysis can develop into an important technique for examining the morphology of polymeric blends. In order to relate dielectric results on polymer systems to statements about the morphology, the use of mixture theories is necessary. There are many of such theories described in the literature (Van Beek,[34] Bánhegyi[17]), all making different assumptions about the validity of the formulas. However, all theories have in common that they use a shape or depolarization factor in order to relate the shape of the particles in the blend to the dielectric response. The shape factor of an ellipsoidal particle is given by, e.g., Van Beek.[34] It is possible to describe a fiber as an ellipsoid in which the two short axes are equal and the long axis is infinite. However, it is not possible to describe a fiber during the breakup process as an ellipsoid. Therefore, we have to derive a new relation for the shape factor of the distorted fiber.

The classical description of the breakup of liquid threads embedded in an immiscible matrix was first given by Lord Rayleigh[30] and extended by Tomotika[31,32] for Newtonian fluids. They assumed the thread to exhibit an axisymmetric distortion. The radius of the distorted thread ($R(z)$) at distance z along the long axis can be written as (Figure 1):

$$R(z) = \bar{R} + \alpha \cos\left(\frac{2\pi z}{\lambda}\right) \tag{1}$$

in which $\bar{R}$ is the average radius of the thread (m), α is the distortion amplitude (m) and λ is the wavelength of the distortion (m). The average radius of the thread can be written as $(R_0^2 - {}^1/_2\alpha^2)^{1/2}$, where R_0 is the initial radius of the thread (m). The breakup of the fiber can be characterized by an increase in the distortion amplitude with time ($\alpha = \alpha_0 e^{qt}$, in which q is the growth rate and t is time).

We now have to calculate the shape factor of the fiber with this cosine-like distortion. The samples we will use in our experiments consist of fibers lined up in a matrix. The fibers will be oriented parallel to the electrodes and consequently have their long axis perpendicular to the electric field. Therefore we only have to determine the shape or depolarization factor perpendicular to the long axis of the inclusions. The depolarization factor (A_k) determines the electric field inside the particle caused by the polarization of the system. Landau and Lifshitz[35] proved that the electric field inside an ellipsoidal particle in a homogeneous external field is also homogeneous. We assume that the electric field inside a distorted fiber is likewise homogeneous.

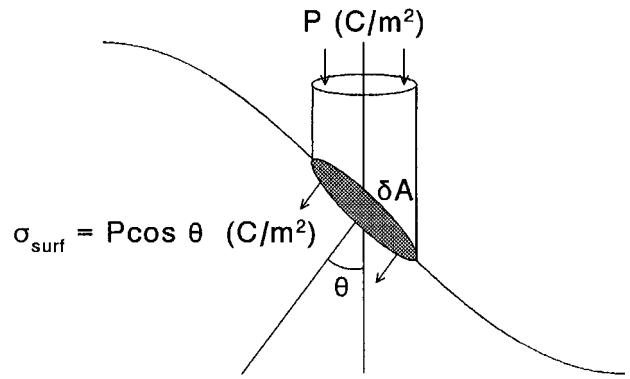

Figure 2. Detail of the surface of a fiber for the calculation of the charge density on its surface, σ_{surf}.

As a result we only have to calculate the electric field at a single point inside the fiber. Considering a particle in a matrix, an effective polarization charge will accumulate at the boundary if the permittivities and conductivities of the phases are different. The relation between the induced electric field inside the particle and the polarization of the system can be given by

$$E_{pol} = \frac{P}{\epsilon_0} A_k \tag{2}$$

P is the effective polarization at the interface between the phases (C/m^2), E_{pol} is the electric field inside the particle caused by the polarization (C/m), and ϵ_0 is the permittivity of vacuum (8.854×10^{-12} F/m). We now have to relate the factor A_k to the shape of the particle. The electric field of a charge Q (C) at a distance r (m) can be written by

$$E_Q = \frac{Q}{4\pi\epsilon_0 r^2} \tag{3}$$

The polarization charge is not located at one point on the surface of the particle but is spread out over the entire surface; therefore we have to integrate over this surface. The charge Q must be replaced by the charge density on the surface (σ_{surf}) times an infinitesimal small surface element (dA). We want to calculate the electric field at point 0 (Figure 1). If we assume that the particle is symmetrical in the y and z directions, we only have to use the x-component (in the direction of the external electric field) of the charge in our calculations ($=\sigma_{surf} dA x/r$). The charge density on the surface of the particle can be derived from the polarization in the x-direction (P) corrected for a larger surface area ($\sigma_{surf} = P \cos\theta$, Figure 2).

We now have to integrate over the entire surface:

$$E_Q = \frac{P}{4\pi\epsilon_0} \int_A \frac{x}{r^3} \cos\theta \, dA \tag{4}$$

x is the x-component of a point on the surface and can be written as $R(z)\cos\beta$, the distance r can be written as $(R(z)^2 + z^2)^{1/2}$, the cosine of the angle between the x-axis and the normal of the surface (θ) is

$$\cos\theta = \frac{\cos\beta}{\sqrt{1 + \left[\frac{\partial R(z)}{\partial z}\right]^2}} \tag{5}$$

dA is a small surface element of the particle: $dA = R(z)d\beta(1 + (\partial R(z)/\partial z)^2)^{1/2}dz$. E_{pol} must be equal to E_Q. The electric field is directed along the x- or b-axis. The

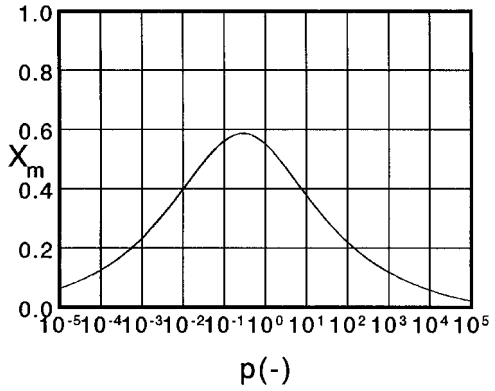

Figure 3. Dominant wave number, $X_m = 2\pi R_0/\lambda_m$, as a function of the viscosity ratio of the two polymers, $p = \eta_{fiber}/\eta_{matrix}$.

calculated shape factor is therefore also along the *b*-axis. The general shape factor A_k must be replaced by the shape factor along the *b*-axis A_b. The resulting integral becomes

$$A_b = \frac{1}{4\pi}\int_{-\infty}^{\infty}\int_0^{2\pi}\cos^2\beta\,\frac{R^2(z)}{(R^2(z)+z^2)^{3/2}}\,d\beta\,dz = \frac{1}{4}\int_{-\infty}^{\infty}\frac{R^2(z)}{(R^2(z)+z^2)^{3/2}}\,dz \quad (6)$$

For spheroidal particles, in which $R(z) = b(1 - z^2/a^2)^{1/2}$, eq 6 can be solved by integrating from $-a$ to a. This yields the shape factor along the *b*-axis for prolate spheroids given, e.g., by Van Beek.[34]

$$A_b = \frac{1}{2}\left[1 + \frac{1}{n^2-1} - \frac{n}{(n^2-1)^{3/2}}\ln[n + \sqrt{(n^2-1)}]\right] \quad (7)$$

in which n represents the ratio between the long axis (a) and the short axis (b) of the spheroid ($n = a/b$).

In our case, when we substitute eq 1 into eq 6, there is no analytical solution known for the integral. Therefore, we have to use numerical methods to evaluate eq 6. The results of the numerical integration depend on the initial values of λ and R_0. The wavelength by which the polymer fiber will break up depends on the viscosity ratio of the two components ($p = \eta_{fiber}/\eta_{matrix}$). The growth rate of the distortion shows a maximum at one wavelength (the dominant wavelength λ_m). Machiels[25] showed that for large initial distortions (e.g., $\alpha_0 = 0.1R_0$) there is a broad area around the dominant wave number X_m ($=2\pi R_0/\lambda_m$) where the breakup time is roughly the same. Therefore, the fiber will not break up with one wavelength, but with a distribution of wavelengths. For small values of the initial distortion (e.g., $\alpha_0 = 0.001R_0$) the breakup time has a relatively sharp minimum at the dominant wave number. The fibers in our experiments were relatively thick (ca. 100 μm). The initial distortion will, therefore, be small compared to the fiber diameter. Hence, in our calculations, we assume that the fiber will break up at the dominant wave number. The dominant wave number depends on the viscosity ratio of the polymers (p). This is shown in Figure 3.

We can substitute for λ in eq 1 $\lambda = 2\pi R_0/X_m$. The value of X_m can be found from Figure 3 for a given viscosity ratio p. By dividing the numerator and denominator of eq 6 by $\bar{R}^3$, the resulting equation for the depolarization factor becomes

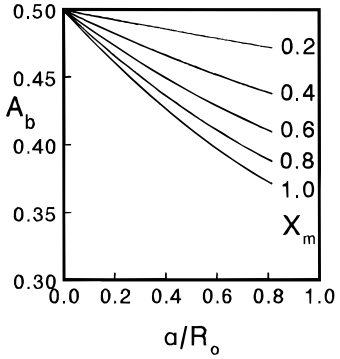

Figure 4. Shape factor of distorted fibers along their short *b*-axis as a function of the relative distortion, α/R_0, for a number of values of the dominant wave number X_m.

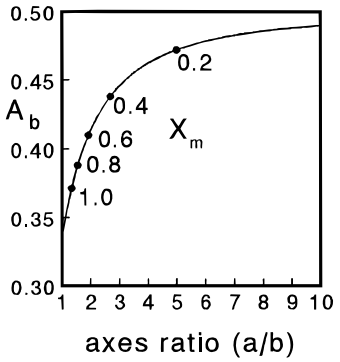

Figure 5. Shape factor of an ellipsoidal particle along its *b*-axis as a function of the ratio between the long and short axes ($a/b = n$). The points on the line indicate the shape factor immediately after breakup (i.e., $\bar{R} = \alpha = 0.82R_0$) at different values of the dominant wave number, X_m.

$$A_b = \frac{1}{2}\int_0^{\infty}\frac{\left[1 + \frac{\alpha}{\bar{R}}\cos\left(X_m\frac{z}{R_0}\right)\right]^2}{\left[\left[1 + \frac{\alpha}{\bar{R}}\cos\left(X_m\frac{z}{R_0}\right)\right]^2 + \left[\frac{z}{\bar{R}}\right]^2\right]^{3/2}}\frac{1}{\bar{R}}\,dz \quad (8)$$

The numerically derived graphs of A_b for a number of values of X_m are shown in Figure 4 as a function of the relative distortion amplitude (α/R_0). If the value of α is equal to the average radius of the fiber ($\bar{R} = 0.82R_0$), the fiber is assumed to be broken up. The resulting particle is a spheroid with its short axis equal to $2\bar{R}$ ($=1.64R_0$). Its long axis can be calculated from the shape factor at the time of breakup. This particle will in turn retract to a spherical-shaped particle. The evolution from a spheroid to a sphere is shown in Figure 5. The points on the solid line are the shape factors at corresponding axes ratios (a/b) of the particle immediately after breakup for different values of the dominant wavenumber (X_m). The diameter of the resulting sphere is $R_0(12\pi/X_m)^{1/3}$.

Application of Existing Mixture Theories. In the previous section we derived a relation between the depolarization or shape factor and the actual shape of the distorted fiber. In order to relate the dielectric data to values for the shape factor, we need a mixture theory which describes our measurements in the best way possible. There are a lot of mixture theories known in the literature. Most of them are summarized in the articles by Bánhegyi.[14,15,17] The problem, however, is that there is not one theory that covers all experiments. The existing mixture theories can be divided into matrix-inclusion and statistical mixture types. In the case of fibers in a matrix, without percolation, the matrix-inclusion types are preferred. The simplest

theory is the Maxwell−Wagner−Sillars[36] theory:

$$\epsilon^* = \epsilon_1^* \frac{\epsilon_1^*(1-\phi_2)(1-A_k) + \epsilon_2^*(\phi_2 + A_k(1-\phi_2))}{\epsilon_1^* + A_k(1-\phi_2)(\epsilon_2^* - \epsilon_1^*)} \quad (9)$$

In which ϵ_1^*, ϵ_2^*, and ϵ^* are the complex permittivities of, respectively, the matrix, the inclusions, and the blend, and ϕ_2 is the volume fraction of the inclusions. This theory is only valid for low volume fractions of the dispersed phase. Therefore the simple theory of Maxwell−Wagner−Sillars cannot be used for higher volume fractions.

A second group of formulas is based on the integration technique. A well-known theory in this group is the Bruggeman−Boyle[37] theory for oriented inclusions, which is derived through integration of the Maxwell−Wagner−Sillars equation to higher volume fractions.

$$\left[\frac{\epsilon^* - \epsilon_2^*}{\epsilon_1^* - \epsilon_2^*}\right]\left[\frac{\epsilon_1^*}{\epsilon^*}\right]^{A_k} = (1-\phi_2) \quad (10)$$

The last group of mixture theories is the statistical mixture type. These models assume that the ellipsoidal particles are embedded in an effective medium. The most important formula was derived by Böttcher,[38] extended by Polder and Van Santen[39] for randomly oriented ellipsoids and later by Hsu[40] for oriented ellipsoidal particles:

$$\frac{(\epsilon_1^* - \epsilon^*)\phi_1}{\epsilon^* + (\epsilon_1^* - \epsilon^*)A_k} + \frac{(\epsilon_2^* - \epsilon^*)\phi_2}{\epsilon^* + (\epsilon_2^* - \epsilon^*)A_k} = 0 \quad (11)$$

in which ϕ_1 is the volume fraction of the matrix. It is difficult to predict which mixture theory can be used best in our experiments. Therefore, we have performed some measurements to discriminate between the three formulas.

III. Experiments

Materials. The samples for breakup experiments consisted of Vectra B950 fibers embedded in a polypropylene matrix. Vectra B950 is a random copoly(esteramide), consisting of 60% 2,6-hydroxynaphthoic acid, 20% terephthalic acid, and 20% aminophenol, supplied by Hoechst-Celanese. The as-received granules were dried at 180 °C for 4 h in a nitrogen atmosphere and kept under vacuum at 60 °C afterward. DSC showed that the melting point of the granules was about 284 °C. The Vectra B950 granules were made into a fiber by melting them in a capillary rheometer at 300 °C. The polymer thread from the capillary (diameter 1.5 mm, length 50 mm) was drawn and yielded fibers with a diameter of about 100 μm. The polypropylene used was Stamylan P 13E10 supplied by DSM. The fibers were lined up and embedded in the matrix by compression molding between two films of PP at 230 °C. The resulting film thickness was between 300 and 400 μm. The volume fraction of the resulting samples varied between 4 and 15%.

Dielectric and Optical Measurements. The breakup experiments were performed in two ways. The first experiments were done at 300 °C in a Mettler FP80 HT hot stage mounted under an optical microscope (Jenapol). The samples were put between two ITO-coated glass plates. Quartz fibers kept the distance between the electrodes constant during the measurements. The ITO layers were connected to the dielectric equipment. In this way it was possible to perform simultaneously optical and dielectric measurements. The dielectric measurements were performed using a Hewlett-Packard 4284A precision LCR-meter. The frequency range used was 32 to 500.000 Hz.

A second series of experiments was done inside a dielectric sample holder (Willems[41]). Circular samples (3 cm in diameter) were placed between two circular quartz plates of 4 cm in diameter. A gold electrode of 3 cm in diameter was sputter coated on each quartz plate. The two electrodes on each plate were connected to the dielectric analyzer. A spacer ring of polyimide film (Kapton) around the sample kept the electrodes at a constant spacing. The sample holder was placed inside a Novocontrol temperature control unit, which regulated the temperature by means of a heated nitrogen flow. The dielectric measurements were made using the HP LCR-meter for high frequencies (1−500 kHz) and a combination of a Schlumberger SI 1260 frequency response analyzer and a dielectric electrometer (TNO) for low frequencies (0.5−1000 Hz). The breakup experiments inside the sample holder were also performed at 300 °C.

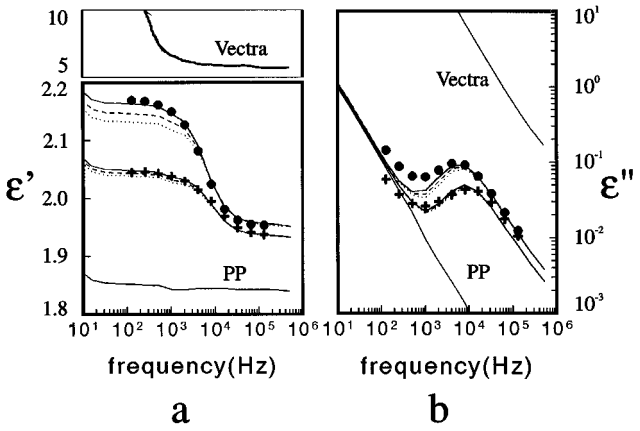

Figure 6. Permittivity (a) and dielectric loss (b) vs frequency of pure Vectra B950 and polypropylene and a 4.8 vol % sample. Measured data: (+) $A_b = 1/2$ (fiber); (●) $A_b = 1/3$ (sphere). Calculations according to (—) Böttcher−Hsu; (---) Bruggeman−Boyle; (···) MWS.

Scanning Electron Microscopy. The sample morphologies were analyzed using a Philips XL 20 scanning electron microscope. On the assumption that the distribution of the fibers was homogeneous throughout the sample, we could derive the volume fraction of the solid sample from the area ratio between the cross section of the fibers and the total sample. The volume fractions of the samples during the measurements were more difficult to obtain, because of the molten state of the samples. They could be calculated from the volume fractions in the solid state using the densities of the polymers at 300 °C. Since this calculation was not very accurate, we derived the volume fractions from the dielectric measurements.

IV. Results and Discussion

Discrimination between Mixture Formulas. We started our experiments by performing dielectric measurements on films of pure polypropylene and Vectra B950 inside the dielectric sample holder. The measured permittivity (ϵ') and dielectric loss (ϵ'') of the pure components are plotted in Figure 6. Next, we used eqs 9−11 to calculate the dielectric response for fibers ($A_b = 1/2$) and spheres ($A_b = 1/3$) for the three different theories. These curves are also plotted in Figure 6. It is obvious that there is a significant difference between the three models. The marked dots in Figure 6 represent the measured results of Vectra B950 fibers in a polypropylene matrix (4.8 vol %) before ($A_b = 1/2$) and after ($A_b = 1/3$) breakup. It is clearly visible that the Böttcher−Hsu model describes the experimental data better than the other two models. We noticed that the other experiments in this paper were also better described by the Böttcher−Hsu model. Therefore, all our calculations were performed using this model. The volume fractions of the samples were calculated from the first frequency scan, with the knowledge that the shape factor of the undistorted fiber equals 1/2.

Electrode Effects. When observing the real permittivity of pure Vectra B950 in Figure 6, we notice an

increase at low frequencies. This is caused by the appearance of electrode polarization. It is well-known from the literature that dielectric measurements on conductive samples can show electrode polarization. This polarization can be oppressed by, for example, increasing the sample thickness. In the case of our polymer composites, it was not necessary to adjust the sample configuration, because the conductivity of the matrix was too low to cause electrode polarization at the dispersion frequencies. Therefore, our measurements are not significantly influenced by any electrode effects.

Data Analysis. All our measurements yield plots of permittivity and loss against frequency at 300 °C. A frequency scan took, depending on the number of frequencies, between 90 and 200 s. During this time the breakup process was proceeding. Therefore, the calculated shape factor did not correspond to the shape at the beginning of the scan, but to the shape halfway through the frequency scan. In a next publication (Boersma[29]) we will reduce the number of frequencies in order to get a more accurate shape factor at a particular time. By reducing the number of frequencies, the number of scans will increase and this will result in more measurement points during the breakup process.

The dielectric data were fitted over the entire frequency range. For measurements with strong deviations in the loss curves (i.e., the measurements under the optical microscope), we used only the values of the real part of the permittivities in the fit procedure. This resulted in rather good fitting results for all the measured data points. The data were fitted using a rearrangement of the Böttcher−Hsu equation (11):

$$\epsilon^* = \epsilon^*_{\text{matrix}} + (\epsilon^*_{\text{fiber}} - \epsilon^*_{\text{matrix}})\phi_{\text{fiber}} \frac{\epsilon^*}{\epsilon^* + (\epsilon^*_{\text{fiber}} - \epsilon^*)A_k} \quad (12)$$

which can be rewritten in the following expression for A_k:

$$A_k = \frac{\epsilon^*((\epsilon^* - \epsilon^*_{\text{matrix}}) - \phi_{\text{fiber}}(\epsilon^*_{\text{fiber}} - \epsilon^*_{\text{matrix}}))}{(\epsilon^* - \epsilon^*_{\text{matrix}})(\epsilon^* - \epsilon^*_{\text{fiber}})} \quad (13)$$

The fit procedures were performed with the help of the mathematical software MapleV3 from Waterloo Maple Software.

Breakup Experiments under an Optical Microscope. In order to relate dielectric measurements during the breakup of polymer fibers with the actual morphology of the blend, we have performed breakup experiments under an optical microscope. In this way we could simultaneously follow the actual breakup process and perform dielectric measurements. Due to contact problems between the ITO electrodes on the glass plates and the dielectric equipment, the values of the permittivity and loss at low frequencies (below ca. 500 Hz) were not very accurate. Therefore, we have not used these values in our data analysis. The experimental setup also caused the values of the loss at low frequencies to show spurious conduction.

Figure 7 shows a dielectric measurement of a breakup experiment of a 4.8 vol % blend of Vectra B950 fibers in polypropylene. The marked dots are the actual measured points and the solid lines are the fitted values. The only fit parameter is the shape factor of the inclusions. The calculated shape factors are plotted in Figure 8, together with two other measurements on the same sample. The calculated values of the shape factor can be converted to the actual shape of the fiber using eq 8. The shape factor A_k of eq 13 is along the *x*- or *b*-axis and is therefore equal to A_b in eq 8. We used the numerically derived curves of A_b versus α/R_0 of Figure 4 to convert A_b into α/R_0. We have to bear in mind that the calculated shape of the fibers is of a sinusoidal type, because we assumed that the fibers break up in this way. This might not be exactly true, since other breakup schemes have been found as well. The conversion of A_b to actual particle shapes after the fibers were broken up has been done using eq 7. We have used the average values of the three experiments in Figure 8 to calculate the shape of the fibers during the breakup process.

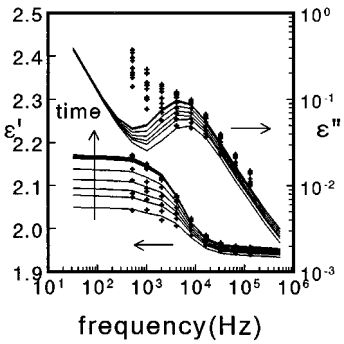

Figure 7. Permittivity and dielectric loss during the breakup process of Vectra B950 fibers in a polypropylene matrix (4.8 vol %) at 300 °C. The markers represent the measured data. The solid lines represent the fitted values.

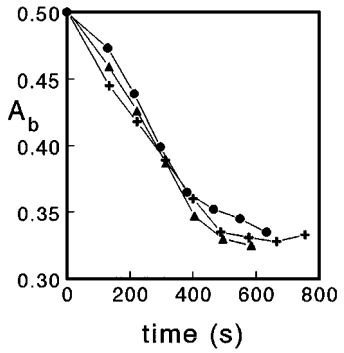

Figure 8. Calculated change in shape factor vs time for three similar samples (4.8 vol %), whereby ● pertain to the measured data of Figure 7.

Rheological experiments showed that at 300 °C the viscosity of Vectra B950 at low strain rates (0.1 s^{-1}) is approximately 400 Pa·s (Beekmans[42]). The viscosity of the polypropylene is approximately 1400 Pa·s under these conditions (Machiels[25]). The viscosity ratio in our experiments was therefore ca. 0.3, which gives a value for the dominant wave number (X_m) of about 0.6.

Photographs were taken every 90 s after the start of the experiment. Therefore, we had to interpolate between the measured points in the shape factor vs time curve (Figure 8). Using these values of the shape factor and assuming for X_m a value of 0.6, we could determine the gradual change in the shape of the fiber using eq 8 and the shape of the spheroids using eq 7. Figure 9 illustrates the procedure of the data evaluation. This figure also includes a series of micrographs of one of the breakup experiments shown in Figure 8. Data points corresponding to Figure 9 and calculated values for α/R_0 and n are listed in Table 1.

Although the fiber breakup process of the model system studied does not behave according to a pure

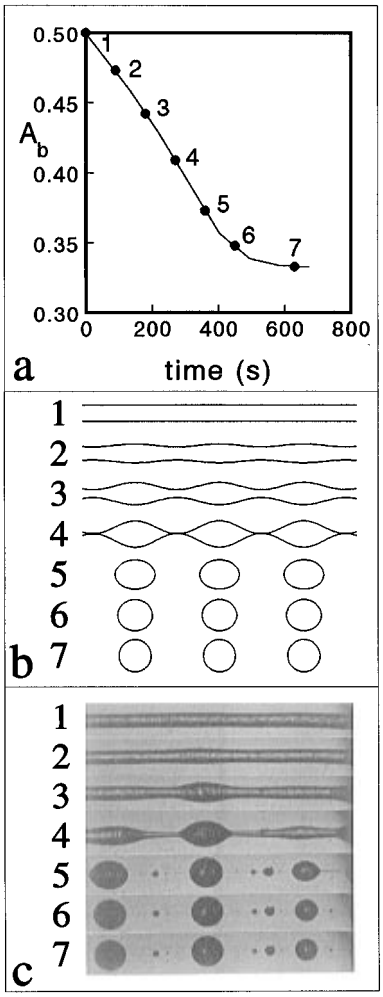

Figure 9. Shape factor (a), calculated shape (b), and actual shape (c) vs time during the breakup of a Vectra B950 fiber in a polypropylene matrix at 300 °C.

Table 1. Calculated Relative Distortion Amplitudes (α/R_0) and Axis Ratios $n(a/b)$ for Measured Values of the Shape Factor (A_b) (See Figure 9)

no.	A_b	a/R_0	n
1	0.500	0	
2	0.476	0.181	
3	0.444	0.453	
4	0.410	0.810	
5	0.373		1.37
6	0.348		1.12
7	0.333		1

Rayleigh breakup mechanism, the predicted shapes at the different stages in the process correspond quite well with the photographs. We cannot predict the formation of the small droplets between the larger ones, because these are not included in the Rayleigh model. Besides, the dielectric technique takes a volume average over the sample and the volume fraction of these droplets is too small to be significant in the measurement.

Breakup Experiments inside the Dielectric Sample Holder. The dielectric measurements under the optical microscope had the disadvantage that, due to the experimental setup, the values of the loss at low frequencies were not very accurate. This was caused by the conductivity of the glass substrate of the ITO electrode. To improve the accuracy of the measurements, we performed another series of experiments using the temperature controlled dielectric sample holder. The measurements could now be extended to lower frequencies.

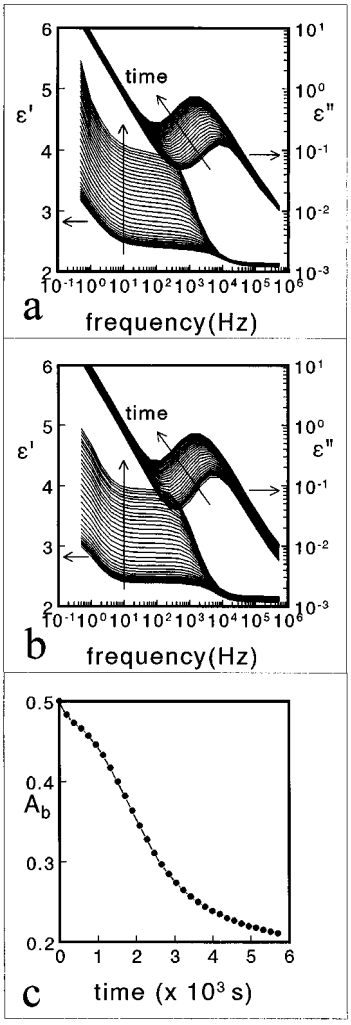

Figure 10. Permittivity and dielectric loss during the breakup of Vectra B950 fibers in a polypropylene matrix (11.2 vol %): experimental data at 300 °C (a), fitted curves (b), and obtained time dependence of shape factor (c).

Figure 10a shows the permittivity and loss of a 11.2 vol % sample during breakup. The fitted curves of this experiment are shown in Figure 10b (only the frequencies between 32 and 125 000 Hz were used in the fit procedure). The values obtained for the shape factor are shown in Figure 10c. As expected, there is a gradual decrease in the shape factor, it even drops below $^1/_3$. The latter is surprising because the expected minimum value of the shape factor is $^1/_3$ (sphere). A decrease below this value means that the change of the shape of the particle did not end in a sphere, but shifted beyond. This drop in value of the shape factor below $^1/_3$ occurred only in samples with volume fractions higher than ca. 8%. It appeared to be the result of the sample preparation. The samples consisted of only one layer of Vectra B950 fibers between two films of polypropylene. In order to increase the volume fraction, the fibers had to be placed closer together. The optical microscope revealed that fibers which lay close to each other coalesce during melting and breakup. This coalescence produced larger particles than one would expect from the size of the original fibers. Therefore, the diameter of the resulting spheres exceeded the electrode spacing. The particles were consequently squeezed between the electrodes which resulted in flattened spheres. Consequently, the resulting system could not be described simply by the two-phase model of particles in a matrix. It had to be described by a pure Vectra B950 phase

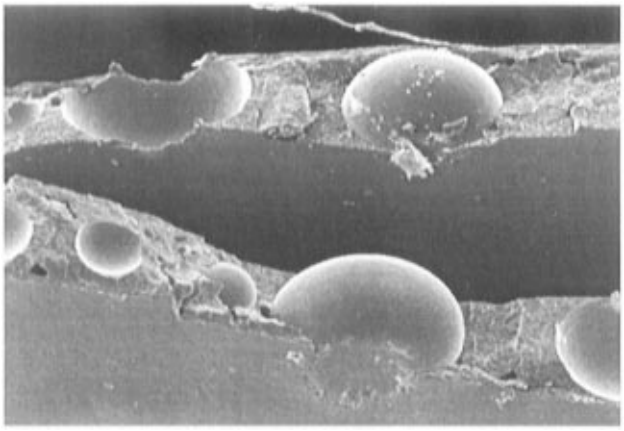

Figure 11. Scanning electron microscope micrograph of the sample of Figure 10 after breakup of the LCP fiber.

parallel to a polypropylene matrix containing Vectra B950 particles. SEM micrographs (Figure 11) indeed demonstrate the existence of flattened particles in this system. Because of this, it was impossible to convert the calculated shape factor into actual shapes of the particles.

In order to do measurements on samples with higher volume fractions, we had to distribute the fibers over the entire matrix and not only in a single layer. We achieved this by stacking three fiber-containing films crosswise together (inset, Figure 12c). Figure 12 shows the results of a 9.3 vol % sample. The shape factor did not drop below $^1/_3$ anymore, which indicated a smooth breakup process from fibers to spheres. This is also demonstrated by the SEM micrographs in Figure 13.

Comparison of the Breakup Experiments. The increase in the distortion amplitude with time ($\alpha = \alpha_0 e^{qt}$) characterizes the breakup process. The initial distortion amplitude (α_0) has a large influence on the breakup process but is very difficult to measure. The value is determined for instance by the initial smoothness of the fiber or stress and orientation in the fiber. The growth rate (q) depends on the interfacial tension between the two phases, the viscosity of the matrix, the viscosity ratio between the dispersed and continuous phase, and the radius of the initial fiber. In our experiments, only one parameter was varied, i.e. the radius of the fibers.

The changes in shape factor of fibers in four different breakup experiments are shown in Figure 14a. The shape factors of the low volume fraction samples (S1 and S3, 4.8 vol %) shifted from $^1/_2$ to $^1/_3$. The samples with higher volume fractions (S2, 14.4 vol %, and S4, 9.8 vol %) showed a shift from $^1/_2$ to values below $^1/_3$. This was caused by the formation of a parallel Vectra B950 fraction in the sample. Samples S1 and S2 were measured between the ITO glass plates under the microscope, S3 and S4 were measured in the dielectric sample holder. It is clearly visible that the breakup process of the samples under the microscope is faster than in the sample holder. This is caused by the higher heating rate inside the hot stage. As a result, the Vectra B950 fibers had less time to lose their orientation and built-in stresses. The initial distortion amplitude was therefore higher than at lower heating rates.

Comparison between the low and high volume fraction curves shows that fibers of a low volume fraction sample break up faster than fibers of a higher volume fraction sample. This is caused by coalescence of the fibers, which resulted in fibers with a larger diameter and a slower breakup process. Another presentation of

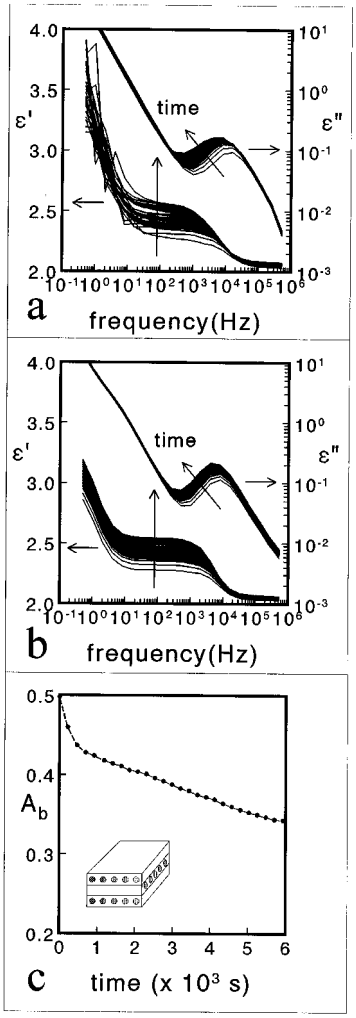

Figure 12. Permittivity and dielectric loss during the breakup of fibers in a laminate of three fiber-containing films (9.3 vol %): measured data (a), fitted curves (b), and obtained change in shape factor with time (c). The fibers are stacked crosswise (c, inset).

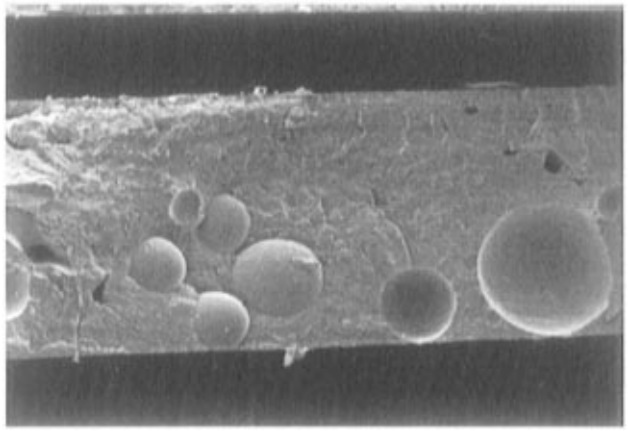

Figure 13. SEM picture of the sample of Figure 12 after breakup of the LCP fiber.

the same data is shown in Figure 14b, which gives the logarithm of the relative distortion amplitude against time. The maximum value of α/R_0 is 0.82 because at this point the fibers break up. The slope of the curves represents the growth rate of the distortion (q). Only the first part of the curves (below ca. $\alpha/R_0 < 0.5$) is significant, because above this value the distortion deviates from the Tomotika theory. This means that in our experiments only the first 250 s can be used to

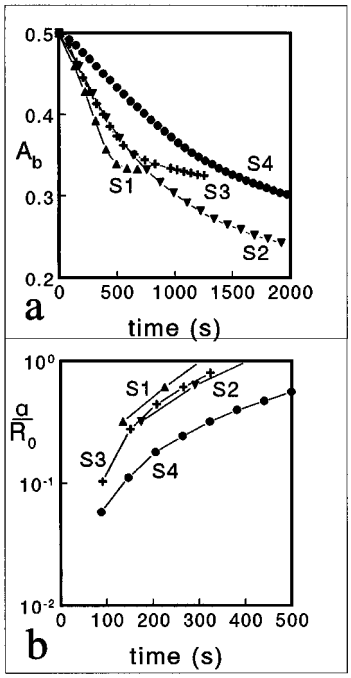

Figure 14. Time dependence of shape factor (a) and calculated relative distortion amplitude (b) of two samples under the optical microscope (S1 (4.8 vol %) and S2 (14.4 vol %)) and two samples in the dielectric sample holder (S3 (4.8 vol %) and S4 (9.8 vol %)).

calculate the growth rate. We already stated that a complete frequency scan takes at least 90 s. It is therefore not possible to do more than three frequency scans at the beginning of the experiment. This problem can be solved by not scanning the whole frequency range, but only two frequencies. These frequencies must be above and below the step in permittivity (for example 500 and 100 000 Hz). The use of only two frequencies shortens the scan considerabely, which makes it possible to perform more measurements in the first part of the breakup experiment. This will be discussed in a forthcoming publication (Boersma[29]).

V. Conclusions

Dielectric measurements on a model system of lined up LCP fibers in a thermoplastic matrix above the melting point of both phases reveal the existence of a strong interfacial polarization. We have shown that this polarization allows one to calculate the shape of the fibers during the breakup. The simplest theory of fiber breakup (by Lord Rayleigh and Tomotika) could be used to convert the shape factor, obtained from our measurements, to distortion amplitudes of the fiber during breakup. The overall breakup behavior of Vectra B950 fibers in a polypropylene matrix can thus be described by a Rayleigh-type distortion, whereas individual fibers might show a different breakup mechanism. A higher heating rate results in a faster breakup, because the built-in stresses and orientation get less time to relax. Samples with a high volume fraction show slower breakup behavior, because neighbouring fibers can coalesce during melting, which results in thicker threads.

The experiments in this paper demonstrate that dielectric spectroscopy is a useful tool for an analysis of the morphology of polymer blends.

Acknowledgment. This work was sponsored by the Netherlands Organization of Scientific Research (SON/STW-NWO).

References and Notes

(1) Crevecoeur, G.; Groeninckx, G. *Bull. Soc. Chim. Belg.* **1990**, *99* (11&12), 1031−1044.
(2) Roetting, O.; Hinrichsen, G. *Adv. Polym. Technol.* **1994**, *13* (1), 57−64.
(3) Qin, Y. *Polym. Adv. Technol.* **1996**, *7*, 151−159.
(4) Heino, M. T.; Hietaoja, P. T.; Vainio, T. P.; Seppälä, J. V. *J. Appl. Polym. Sci.* **1994**, *51*, 259−270.
(5) O'Donnell, H. J.; Baird, D. G. *Polym. Eng. Sci.* **1996**, *36* (7), 963−978.
(6) Choy, C. L.; Lau, K. W. E.; Wong, Y. W.; Ma, H. M.; Yee, A. F. *Polym. Eng. Sci.* **1996**, *36* (6), 827−834.
(7) Datta, A.; Baird, D. G. *Polymer* **1995**, *36* (3), 505−514.
(8) O'Donnell, H. J.; Baird, D. G. *Polymer* **1995**, *36* (16), 3113−3126.
(9) Carius, H. E.; Schönhals, A.; Guigner, D.; Sterzynski, T.; Brostow, W. *Macromolecules* **1996**, *29* (14), 5017−5025.
(10) Rellick, G. S.; Runt, J. *J. Polym. Sci., Polym. Phys. Ed.* **1986**, *24*, 280−302.
(11) Rellick, G. S.; Runt, J. *J. Polym. Sci., Polym. Phys. Ed.* **1986**, *24*, 313−324.
(12) Angeli, S. R.; Runt J. *Contemp. Top. Polym. Sci.* **1989**, *6*, 289−299.
(13) Zetsche, A.; Kremer, F.; Jung, W.; Schulze, H. *Polymer* **1990**, *31*, 1883−1887.
(14) Bánhegyi, G. *Colloid Polym. Sci.* **1986**, *264*, 1030−1050.
(15) Bánhegyi, G. *Colloid Polym. Sci.* **1988**, *266*, 11−28.
(16) Bánhegyi, G.; Karasz, F. E.; Petrović, Z. S. *J. Appl. Polym. Sci.* **1990**, *40*, 435−452.
(17) Bánhegyi, G.; Hedvig, P.; Petrović, Z. S.; Karasz, F. E. *Polym. Plast. Technol. Eng.* **1991**, *30* (2&3), 183−225.
(18) Anderson, J. E. *J. Mol. Liq.* **1993**, *56*, 379−398.
(19) Daly, J. H.; Guest, M. J.; Hayward, D.; Pethrick, R. A. *J. Mater. Sci. Lett.* **1992**, *11*, 1271−1273.
(20) Hayward, D.; Pethrick, R. A.; Siriwittayakorn, T. *Macromolecules* **1992**, *25* (5), 1480−1486.
(21) MacKinnon, A. J.; Jenkins, S. D.; McGrail, P. T.; Pethrick, R. A. *J. Appl. Polym. Sci.* **1995**, *58*, 2345−2355.
(22) Dionísio, M. C. S.; Moura Ramos, J. J.; Fernandes, A. C. *J. Appl. Polym. Sci.* **1996**, *60*, 903−909.
(23) Steeman, P. A. M.; Maurer, F. H. J.; van Turnhout, J. *Polym. Eng. Sci.* **1994**, *34* (9), 697−706.
(24) Machiels, A. G. C.; Denys, K. F. J.; van Dam, J.; Posthuma de Boer, A. *Polym. Eng. Sci.* **1997**, *37* (1), 59−72.
(25) Machiels, A. G. C.; van Dam, J.; Posthuma de Boer, A.; Norder, B. *Polym. Eng. Sci.*, in press.
(26) Elmendorp, J. J. *Polym. Eng. Sci.* **1986**, *26* (6), 418−426.
(27) Elemans, P. H. M.; Janssen, J. M. H.; Meijer, H. E. H. *J. Rheol.* **1990**, *34*, 1311−1325.
(28) Watkins, V. H.; Hobbs, S. Y. *Polymer* **1993**, *34* (18), 3955−3959.
(29) Boersma, A.; van Turnhout, J., submitted for publication.
(30) Lord Rayleigh *Proc. R. Soc. (London)* **1879**, *29*, 71−97.
(31) Tomotika, S. *Proc. R. Soc. (London)* **1935**, *A150*, 322−337.
(32) Tomotika, S. *Proc. R. Soc. (London)* **1936**, *A153*, 302−318.
(33) Stone, H. A.; Leal, L. G. *J. Fluid. Mech.* **1989**, *198*, 399−427.
(34) van Beek, L. K. H. *Prog. Dielectrics* **1967**, *7*, 69−114.
(35) Landau, L. D.; Lifshitz, E. M. *Electrodynamics of Continuous Media*; Pergamon: London, 1960; p 42.
(36) Sillars, R. W. *J. Inst. Electr. Eng.* **1937**, *80*, 378.
(37) Boyle, M. H. *Colloid Polym. Sci.* **1985**, *263*, 51−57.
(38) Böttcher, C. J. F. *Recl. Trav. Chim.* **1945**, *64*, 47−51.
(39) Polder, D.; van Santen, J. H. *Physica* **1946**, *12*, 257−271.
(40) Hsu, W. Y.; Gierke, T. D.; Molnar, C. J. *Macromolecules* **1983**, *16* (12), 1945−1947.
(41) Willems, C. R. J. A Dielectric Study of Melting and Crystallization of Semi-Rigid and Flexible-Chain Polymers. Ph.D. Thesis, Delft, 1995.
(42) Beekmans, F.; Gotsis, A. D.; Norder, B. *J. Rheol.* **1996,** *40* (5), 947−966.

MA961794Y